Design considerations for plate and frame ultrafiltration modules by computational fluid dynamics analysis

Dal-Cin, Mauro; Darcovich, Kenneth; Caza, Daniel

Publisher's version / Version de l'éditeur:
https://doi.org/10.1002/cjce.5450840304
Canadian Journal of Chemical Engineering, 84, May 3, pp. 1-2, 2008

Design Considerations for Plate and Frame Ultrafiltration Modules by Computational Fluid Dynamics Analysis†

Mauro M. Dal-Cin*, Ken Darcovich and Daniel Caza

National Research Council Canada, Institute for Chemical Process and Environmental Technology, 1200 Montreal Road, Ottawa, ON, Canada K1A 0R6

Pressure and flow maldistributions were studied in a full-scale industrial plate and frame ultrafiltration module, operating in a Z flow pattern, for the recovery of used motor oils. Solutions were obtained using (1) a three-dimensional solution of the Navier-Stokes equation using computational fluid dynamics and (2) Bernoulli's equation and a momentum balance in one dimension. Fluid decelerations and accelerations generated pressure increases and decreases in the distributor and collector, respectively, biasing the flow distribution to the last channel. Several modifications to the original design were evaluated; the most effective was larger distributor and collector diameters, which greatly improved the uniformity of the flow distribution and transmembrane pressure, and reduced the overall pressure drop in a bank. A variable diameter distributor and collector module was designed using the 1D model. Flow distribution was significantly improved but also yielded an undesirable overall higher pressure drop and a pressure maldistribution in the bank. The maldistribution of the main inlet manifold to the distributors in the first bank was strongly dependent on the module design. The flow distribution across the width of a channel became uniform within a short distance, essentially eliminating the need to consider this design aspect any further. Flows at the bank outlets, and hence inlets of the following bank, showed uniform lateral distribution in all cases, suggesting that future modelling work can be limited to a fraction of the module width, based on symmetry, in order to gain computational efficiency.

Keywords: modelling and simulation, flow and pressure distribution, plate and frame module design, ultrafiltration

INTRODUCTION

This work represents the continuation of a previous study (Dal-Cin et al., 2006) where the pressure and flow distributions in an industrial plate and frame ultrafiltration module were simulated. The motivation for the study was the lack of response of the module's productivity to changes in pressure and average cross flow velocity during the recovery of used motor oil; flow and pressure maldistributions were suspected. Through symmetry, one third of the module width in the first bank was simulated. Thus, an equal flow distribution from the main inlet manifold to each of the 3 distributors across the module width was assumed. Flow and pressure distributions were investigated by two methods. First was a 3D (three-dimensional, computational fluid dynamics) solution of the Navier-Stokes equations with the commercial software, Fluent©. The second method was a spreadsheet solution based on Bernoulli's equation and a momentum balance in one dimension, henceforth, 1D. Solutions to the 1D problem were obtained using an electric circuit analogue, which has been used to model the circulatory system of the human body (Chen et al., 1996,

† *NRCC No. 47872*

* *Author to whom correspondence may be addressed.*
E-mail address: mauro.dal-cin@nrc-cnrc.gc.ca

Tsitlik et al., 1992) as well as pipeline flow (Toldy et al., 1978, Ke and Ti, 2000).

Majumdar (1980) developed a finite-difference model based on a one-dimensional momentum equation and flux continuity for flow along the axis of the plenum, and a Bernoulli type energy balance for velocity components and static pressure in the lateral direction. Dividing and combining manifolds were simulated separately and were not coupled to form a closed system. Heggs and Scheidat (1992) studied the heat transfer and fluid distribution in a 60-channel plate and frame heat exchanger with a Z flow arrangement. Their 1D solution predicted a skewed parabolic flow distribution which, compared to a uniform distribution, varied from −45% at the first channel to 200% at the last channel. The lowest flow rate was located near the inlet but not at the first channel. Similar results were reported by Edwards et al. (1984). Recently, Kee et al. (2002) proposed a generalized model for flow distribution in planar fuel cells, predicting uniform, parabolic or monotonically increasing flow distributions with channel number as a function of dimensionless module and operating parameters.

Our previous 1D and CFD solutions showed that the flow distribution always increased monotonically with increasing channel position, from the inlet, for a module with constant channel, plenum and orifice dimensions. The maldistribution was caused by a pressure increase along the distributor as fluid entered the channels and the fluid remaining in the distributor decelerated. Simultaneously, the pressure decreased along the collector as the average velocity increased. Consequently, the combination of these two pressure distributions generated the greatest pressure drop and flow in the last channel. The flow maldistribution increased as the mean cross flow velocity increased. Maldistribution also worsened with a lower fluid viscosity; the equilibrating back pressure caused by the losses in the channel decreased, as also reported by Edwards et al. (1984).

This work will address the effect of the main inlet manifold, which supplies the feed from a single inlet to the three distributors across the width of the first bank; thus resolving the validity of assuming equally divided flow to each distributor. The maldistribution in the original design was studied at several cross flow velocities revealing deficiencies in the original design. Several different geometric designs of the plate and frame module are simulated to address the pressure and flow maldistributions. The validity of the 1D model, which does not account for the inlet manifold, was further assessed against the CFD solutions as an initial engineering design tool for the different designs.

THE PHYSICAL SYSTEM

The original operating version of the plate and frame module consists of 10 banks with 5 channels per bank. Dimensions and other details are given in Table 1. The general flow path in the main feed inlet, manifold and first bank is best understood by inspecting Figure 1. The main feed enters by a 0.0762 m (3 inch) diameter pipe that goes to a slot manifold that nearly spans the width of the module. In the original design, the feed goes directly out from the full face of the manifold to the first channel whose boundaries are defined by a frame element, Figure 2a. The last channel is also formed by a frame and the directional baffle. The first and last channels have only one permeating wall in this design for a total of 8 permeating walls in the bank. The distributors and collectors are formed by a series of co-linear openings in the plates. Membranes are fastened to the plates using circular clamps that also define the distributor and collector diameters, Dp, and the orifice length, d. The orifice area is defined by

$$A_o = \pi D_p \cdot h \tag{1}$$

where h is the channel gap. Note that Equation 1, in the original design, only applies to channels 2, 3 and 4. The orifice area for channels 1 and 5 is given by

$$2h \times (mw/n + mh). \tag{2}$$

where mw and mh are the manifold width and height respectively and n the number of distributors.

The pressure increases in the distributor and decreases in the collector are caused by changes in fluid velocity in the respective plenums. Reductions in the magnitude of the velocity changes, or a reduction of the inlet feed velocity, can be achieved by several means, such as reducing the number of channels in a bank, using narrower channels, increasing the number of plenums or enlarging the plenum diameters.

Table 1. Design parameters of full scale stack and liquid feed properties

Component	Dimension
Feed inlet/outlet diameter	0.0762 m (3 in)
Inlet manifold, height (mh) x width (mw) x depth (md) (y-x-z in figure 1)	0.0762 × 0.356 × 0.0127 m (3 × 14 × 0.5 in)
Number of collectors/distributors, n	3
Collector/distributor diameter, D_p	0.0349 m (1.375 in) or 0.0508 m (2.0 in)
Channel gap, h	0.00635 m (0.25 in)
Number of channels per bank, n	5
Number of banks	10
Channel width, w	0.40 m
Channel length, l	1.3 m (1.2 m distributor to collector centres)
Plate thickness, L_p	0.0635 m (0.25 in)
Viscosity, μ (@ 70°C)	0.036 kg/m/s
Density, ρ	880 kg/m^3

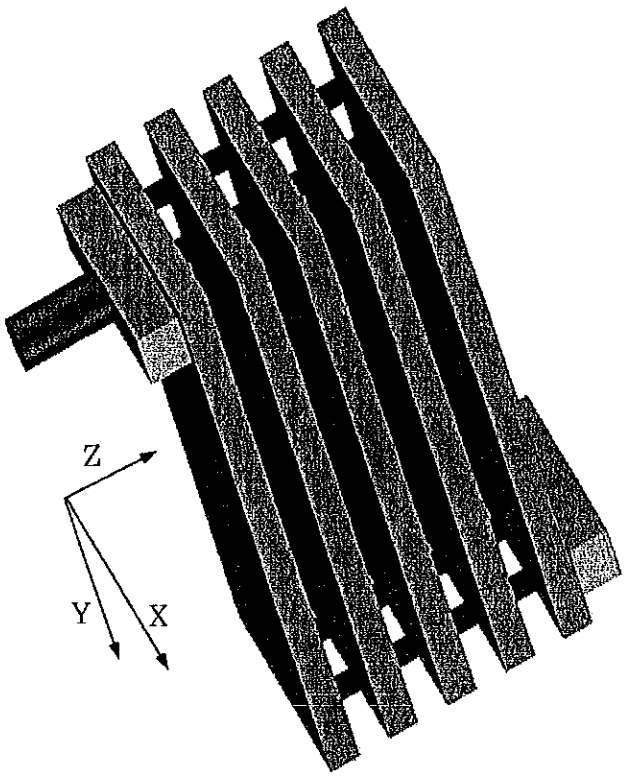

Figure 1. General representation of the volume occupied by retentate in the first bank, showing the inlet manifold and main feed inlet at the upper left. Not drawn to scale for clarity.

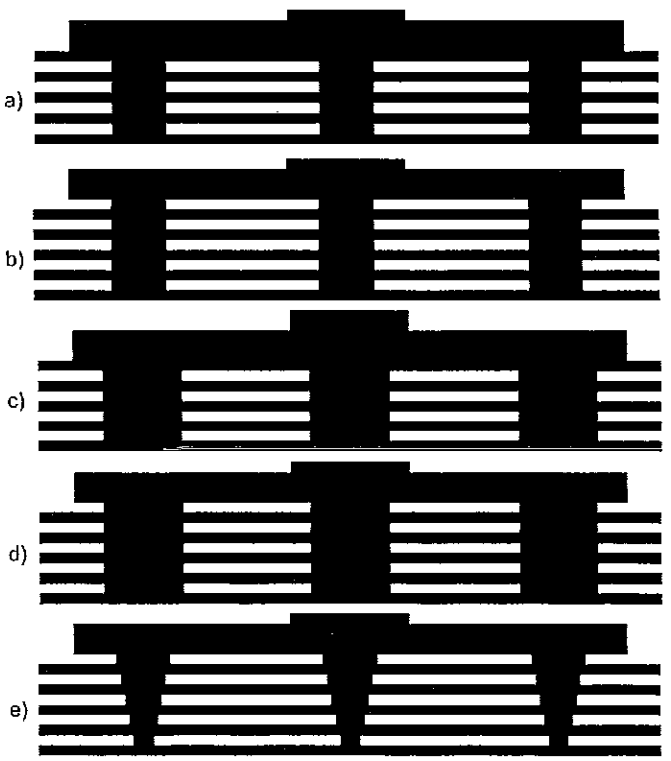

Figure 2. Module designs investigated, (a) original,(b) plates, (c) big plenums, (d) plates and big plenums, and (e) variable plenums, showing cross-sections at the mid-level of the distributor in the x-z plane. Drawn to scale, see text for details.

Reducing the number of channels per bank requires more directional baffles and reduces the packing density of the module with respect to membrane area. The overall module pressure drop could also increase as more banks, and therefore longer flow path, would be needed to maintain a given membrane area. Reducing the channel dimension and maintaining a constant shear rate at the membrane surface would improve the flow distribution by reducing the average velocity at the distributor inlet and increasing the pressure loss in the channels, which would act as means to equilibrate the flows. However, the channel dimension was pre-selected to allow recirculation of a given feed with its particulate loading and viscosity and will be considered a fixed variable for this work.

Increasing the plenum diameters, or number of plenums, are other alternatives. Both are limited by the module width and the latter represents more work during module assembly. The larger diameter approach is preferred as it can allow retrofitting of existing modules. Taking these criteria into account, several modifications to the original design are proposed and simulated.

Details differentiating the various designs are shown in Figure 2 where the cross-sections are defined by the x-z plane in Figure 1 at the midpoint of the main feed tube, manifold and distributors. The original configuration of the industrial unit is shown in Figure 2a. The second, or Plate, design uses a plate element immediately after the slot manifold and just before the directional baffle at the end of the bank, Figure 2b. This results in a constant orifice diameter defined by Equation 1 for all the channels and has 10 permeating walls. Note that this was the design used in the 1/3rd width study (Dal-Cin et al., 2006).

The third, Big Plenums, design is the same as the original but with larger distributor and collector tube diameters, 0.0508 m compared to 0.035 m for the original design, Figure 2c. The fourth, or Plates and Big Plenums, design is a combination of the previous two, Figure 2d, where the orifice area for the first and last channels is defined by Equation 2.

A fifth, Variable Plenums, design, used a different diameter for the distributor and collector for each channel, the dimensions of which were optimized using the 1D model. A logical, but simplistic, first assumption would be that the design would generate a constant average fluid velocity in the distributor and collector. The only pressure changes along the plenums lengths (z-axis) would be due to frictional losses, which are negligible for the short flow path in one bank. The expectation would be a uniform pressure drop across each channel; leading towards a uniform flow distribution. The maximum diameter was restricted to 0.035 m, that of the original design. The diameters of the collector or distributor were the same for all three lateral positions across the width of the channel. This design also used a frame immediately after the inlet manifold and before the directional baffle, Figure 2e. In summary, the different designs are:

- **Original**—Frame at start and end of bank, 0.035 m diameter collector and distributor.
- **Plates**—Plates at start and end of bank, 0.035 m diameter collector and distributor.
- **Big Plenums**—Frame at start and end of bank, 0.0508 m diameter collector and distributor.
- **Plates and Big Plenums**—Combining the previous two modifications.
- **Variable Plenums**—Plates at start and end of bank, variable diameter collector and distributor, limited to a maximum of 0.035 m.

Modelling was simplified with the assumption of a solid wall for the membrane surfaces as the fluxes with oil and the fractional recovery within a bank could be considered negligible. Average fluxes with used motor oil as the feed were $< 3\ L \cdot m^{-2}h^{-1}$ ($4.16 \times 10^{-6}\ m^3 \cdot s^{-1}$). With a permeation area of approximately 5 m^2 per bank, this flux is only 0.032% of the feed rate. Karode (2001) showed that deviations from pressure drops for impermeable walls only became significant with module lengths well beyond those in the plate and frame module and with significantly higher fluxes ($100L \cdot m^{-2}h^{-1}$).

THEORY

1D Simulation

General description and solution method

The 1D solution method and formulations have been previously described in detail (Dal-Cin et al., 2006) and only the general concept is presented here. Flow and pressure distributions were obtained using an electric circuit analogue, the volumetric flow rate and pressure are analogous to the current and voltage respectively. A typical circuit consists of adjacent channels, Figure 3, assuming flow in the direction of increasing channel number and from the distributor to the collector.

Starting immediately after orifice i in Figure 3, the clockwise pressure balance around the loop defined by channels i and $i + 1$ is,

$$\Delta P_{d_{i+1}} + \Delta P_{do_{i+1}} + \Delta P_{channel_{i+1}} + \Delta P_{co_{i+1}} - \Delta P_{c_i} - \Delta P_{co_i} - \Delta P_{channel_i} - \Delta P_{do_i} = 0 \quad (3)$$

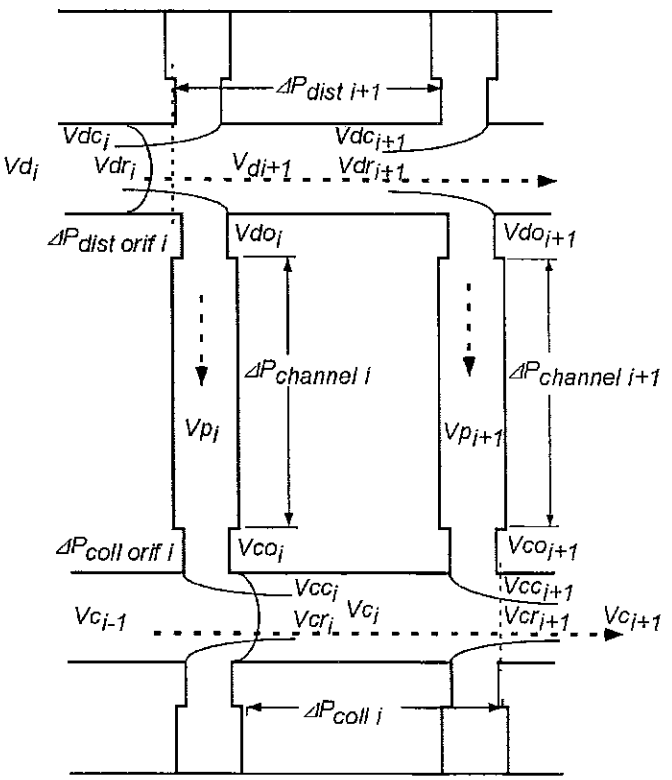

Figure 3. Schematic of flow loop for the ith and i + 1th channels

The positive terms in Equation 3 represent pressure changes in the assumed clockwise flow direction for the (i + 1)st distributor, distributor orifice, channel and collector orifice. The negative terms represent pressure changes opposite the assumed flow direction for the ith collector, collector orifice, channel and distributor orifice.

The solution was obtained by varying the volumetric flow rate in each channel such that the function PE, which we called the pressure error:

$$PE = \sum_{i-1}^{n} (Equation\ 3)^2 \quad (4)$$

was minimized. This forced the pressure loss for the fluid in channels i and $i + 1$ and the associated collector and distributor to be equal, as they must be, under the assumption of no pressure change across the diameter of the distributor or collector. There are $n - 1$ unknown flows in the n channels, the last being known by conservation of mass.

Initial guesses of equal distributions were used for the first four designs where the geometry was fixed and the flows were to be determined. A solution was typically obtained in less than 10 s and with PE < 1 Pa^2 using Microsoft® Excel's (2002 SP-1) add-in solver routine. Boundary conditions were used to limit flows to positive values.

The appropriate pressure loss expressions for laminar or turbulent conditions were used depending on the local Reynolds number. Given the rapidly changing flow directions and short path lengths between channels, flow was assumed to be turbulent in the plenums. In the channels, where the path length was greater than 1 m, the Reynolds number always indicated laminar flow with $N_{Re} = D_h \rho V/\mu < 2\ 000$ at 1 m/s. This and other specific cases are discussed in the Results section. It is recognized that this laminar assumption is an approximation for the 1D model near the distributor and collector as the fluid enters and exits the channel. Issues regarding turbulent-laminar flow transitions in the CFD solution are discussed in the Turbulent to Laminar Transition section.

The variable plenums module was designed assuming a perfect flow distribution in the 5 channels. The solution sought was the distributor diameters before each channel and the collector diameter after each channel. Initial guesses were such that the plenum area decreased/increased by $1/5^{th}$ for the distributor/collector, respectively, after each channel. The solution of this problem was not as robust as the fixed geometry cases. Multiple solutions were obtained, as could be expected given the 10 diameters to be optimized with only four constraining equations; the circuit analogues. The solution which predicted the lowest pressure drop and monotonically decreasing distributor diameters or increasing collector diameters was used as the basis for the CFD simulation.

A ratio of the maximum to minimum flow in any channel, κ_{chan}, is used as an overall measure of the maldistribution in the channels (Jones, 1981). The analogue for the inlet manifold maldistribution, κ_{man}, is the ratio of the maximum to minimum flow into each of the 3 distributors.

3D Simulation

Governing equations

The flow system was governed by equations conserving mass and momentum. At low Reynolds numbers this means respectively that the standard continuity and Navier-Stokes equations

were employed. For turbulent cases the RNG version of the $k-\varepsilon$ model was used as detailed previously (Dal-Cin et al., 2006).

Boundary conditions

Boundary conditions specified at the feed inlet were a $1/7^{th}$ power law velocity distribution and the corresponding turbulent kinetic energy, k, and turbulent dissipation rate, ε, modelled after equations given by Launder and Spalding, (1972). Specifically,

$$I = 0.16Re^{-1/8} \qquad \square = 0.07Di$$

$$k = 1.5(Iu)^2 \qquad \varepsilon = C_\mu \frac{k^{1.5}}{l}$$

Above, u is the fluid velocity normal to the inlet, I is the turbulence intensity, and $\square$ is the turbulence mixing length, given in terms of the inlet diameter D_i.

At the outlet, the gauge pressure was specified to be 0 and the turbulent kinetic energy and turbulent dissipation rate were specified to be the same as at the inlet. Gravitational effects were applied in the x direction.

Computational parameters

Convergence was verified by tracking: (1) residuals of continuity, k, ε, and x, y, and z velocity components; (2) pressure distributions in the distributor and collector centre lines; and (3) the distribution of the average flow in the channels. Pressure and flow distributions were examined at residual maxima starting at 1×10^{-3} and each order of reduction thereafter. Pressure and flow distributions typically stabilized at convergence criteria between 1×10^{-4} and 1×10^{-6}. Convergence was typically achieved between 1 500 and 5 000 iterations with residuals unchanging for at least the final 100 iterations. A first-order downwind, segregated solver scheme was employed.

This simulation treated a system with sharp directional changes and severe geometry variations. In order to minimize convergence instabilities, typical under-relaxation factors of 0.2 were used for continuity, x, y, and z velocity components and 0.5 for k and ε. Periodic convergence behaviour was observed for larger relaxation factors.

Grid considerations

The grid was constructed in Gambit© by first meshing the channel faces (of all 5 channels) that surround the inlet and outlet tubes and then extending the mesh through the channel volume. Each face was meshed by defining nodes along all its edges and allowing Gambit to map the mesh over the face. This was required in order to obtain a well-structured mesh of hexahedra with very low skewness. Highly skewed meshes are known to introduce numerical instability and/or inaccuracy.

Geometric features such as tube sections inside the manifold, which in turn were within a channel face, were meshed in a nested fashion to comprise a full surface in the x-y plane. This allowed sub-elements in any required combination to be projected in the z-direction to build the full module. In this manner the collector and distributors in the variable plenum design were meshed by creating concentric circles in the first channel corresponding to predetermined diameters from the 1D model. The outermost ring was removed after each channel for the distributor, which had decreasing diameters with increasing channel number. The collector diameter increased with channel number, in this case the four outermost rings were removed after the first channel, three after the second channel and so on.

Each channel was divided into three zones for the purposes of meshing. The first zone extends from the top of the channel to 0.08 m past the centre of the distributor. The mesh density in this zone is 0.09 cm to capture recirculation and turbulence effects. The second zone extends from the end of the first zone to 0.08 m before the centre of the collector. The mesh density along the flow direction is 0.9 cm and along the channel gap and width it is 0.09 cm. The flow is fairly consistent in this region, so a less dense grid is able to give satisfactory results. The third zone makes up the rest of the channel in the vicinity of the collector and has the same mesh density as the first zone.

The grid densities employed in the plenums correspond to characterization tests giving good pressure drop predictions in the Reynolds number range being considered here. These separate baseline tests were on straight tubes. This was done because flow fields for turbulent systems are inherently grid dependent, arising from the implementation of wall functions (Manna and Vacca, 2001). Mindful of this, it was appropriate to employ the RNG model, since it is actually less grid dependent than other turbulent models for low-Re turbulence (Rokni and Sundén, 1999). Cui and Kim (2003) investigated grid properties in a turbulent simulation and found that beyond a certain fineness, the quality of the solution deteriorated.

The Plates configuration was used as a test case for grid independence because the smaller plenum diameters produce higher plenum fluid velocities, thus creating larger field gradients. The original Plate configuration mesh had 4.22 million cells. Selective grid refinements in the plenum regions produced a mesh with 9.05 million cells. With this finer mesh, the average change in the flow distribution in the channels was 5%. For the purpose of this work, which was to show the effect of different design configurations, the grid density was considered sufficient.

The full bank width and main feed inlet and manifold were modelled in this work to take into account the horizontal orientation of the module during use and inlet manifold distribution. The effect of gravity was found to be negligible.

Run conditions

High cross-flow velocities were shown to accentuate pressure and flow maldistributions in our previous work. In the current work, the original module design was simulated at 0.5, 1, 2, 3 and 5 m/s. The alternative module designs were evaluated at a typical 1 m/s nominal design cross flow velocity. The boundary conditions for turbulent kinetic energy and turbulent dissipation rate were set accordingly for the main inlet.

Turbulent to laminar transitions

From a trial calculation at the highest mass flow rate, values of $k = 14.66\ m^2/s^2$ and $\varepsilon = 1.3223 \times 10^4\ m^2/s^3$ were extracted from a cell just below the feed tube in the centre of the last channel. In a maldistributed bank, the last channel was found to have the highest flow rate through it. The ratio k/ε gives a characteristic time over which the turbulence should dissipate. When this characteristic time is multiplied by the average velocity in the channel, a characteristic length over which the turbulence will be eliminated can be estimated. For example, at an average fluid velocity of 5 m/s, the turbulence dissipation length was found to be 5.5 mm.

In some real cases however, because of flow maldistribution, the mass flow rate through the last channel at the 5 m/s nominal cross-flow velocity was found to be high enough to produce a turbulent

Table 2. Inlet manifold and channel flow distributions, pressure losses (1) for module and inlet manifold, (2) to manifold outlet, (3) bank alone, (1–3) at 1 m/s nominal cross-flow velocity

Design	κ_{man}	κ_{chan}	ΔP_{module} (kPa)	$\Delta P_{manifold}$ (kPa)	ΔP_{bank} (kPa)
Original	6.17	2.30	40.0	1.9	38.2
Plate	1.41	2.80	49.2	8.1	41.1
Larger Plenums	11.76	1.25	23.8	0.0	23.8
Plate and Larger Plenums	2.70	1.26	26.2	2.3	23.8
Variable Plenum	1.38	1.29	64.2	8.2	56.0

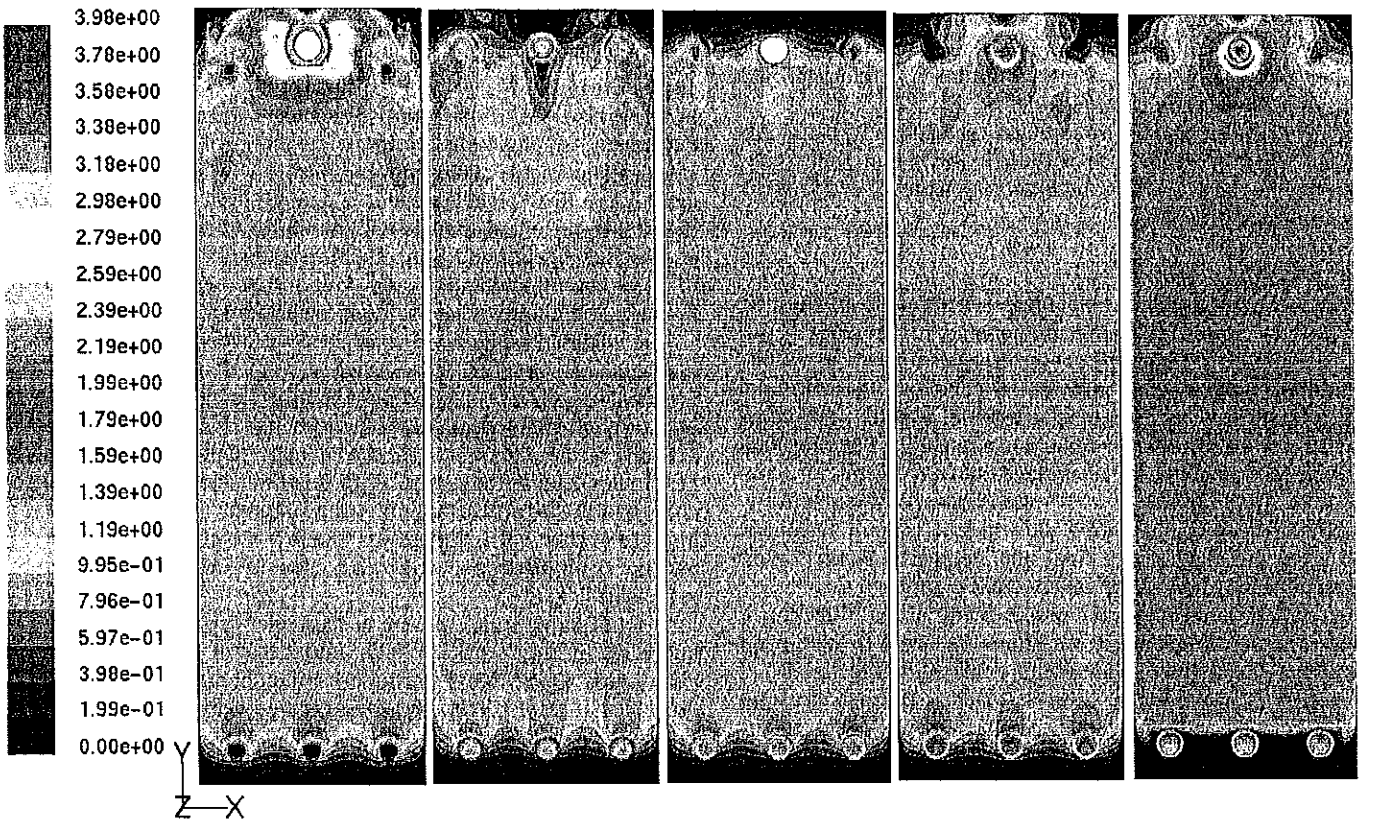

Figure 4. Velocity contours at mid-channel for the large plenum design with poor inlet manifold distribution, channel 1 on left, channel 5 on right

channel Reynolds number. In particular the fourth and fifth channels for the highest inlet velocity case had turbulent flow.

In most cases, the Reynolds number of the flow in the channel indicated a laminar regime. Since no turbulence will be generated under these conditions, the parameters k and ε were found to decay quickly along the channel. Trial calculations indicated that for Re < 500, an essentially laminar character was output by the $k-\varepsilon$ solver. In this way, the functionality of the turbulent parameters maintained a smoothness that would not be possible to achieve if laminar zones were imposed, which would necessarily entail some discontinuity in the solution of field variables. At present, Fluent© cannot support damping functions on turbulent properties.

RESULTS AND DISCUSSION

An assumption in our 1/3rd width simulations was the uniform lateral flow partitioning of the inlet manifold and its effect on the flow and pressure distributions. The efficacy of the inlet manifold will be addressed first, followed by comparisons of flow and pressure distributions in the 1/3rd and full width simulations for the plate design that was used in Dal-Cin et al. (2006).

The effect of the nominal cross-flow velocity on the flow distributions for the original design is then investigated. Analysis and presentation of the different module designs will be facilitated by considering flow and pressure distributions separately, recognizing that the two are in fact linked. A qualitative discussion of pressure and flow maldistribution on ultrafiltration performance is presented.

Comparisons between CFD and 1D simulations are made throughout to further evaluate the 1D model.

Inlet Manifold Maldistribution

Inlet manifold flow distributions with all the designs were biased towards the centre distributor, as would be expected. The side distributors received virtually identical flows. κ_{man} (centre flow/side flow) is summarized in Table 2 for the various module configurations. The large plenum design had the greatest

maldistribution with κ_{man} = 11.76. κ_{man} decreased for any design using smaller plenum diameters or a plate at the start of the bank, that is, any configuration where pressure losses just after the manifold are greater. The lowest κ_{man} = 1.4 was obtained with the two designs using a plate immediately after the slot manifold and the smaller plenum diameter. Inside the channels, the flow distributed quickly across the width, within 10–20 cm downstream of the distributor, even for the worst case of κ_{man} = 11.76 with the Large Plenum design, Figure 4. This may explain the accuracy of the 1D flow distribution predictions in the channels for the 1/3rd width simulations, despite its poor pressure distribution predictions, as will be discussed in the Pressure Losses and Distributions section.

Comparison of 1/3rd and Full Width Simulations

A logical step in modelling ultrafiltration in any geometry is to include solute retention and permeation, which would add considerably to the computational demands (Miranda and Campos, 2001). Therefore, it is desired to obtain computational efficiency through symmetry or simplifying assumptions, such as uniform lateral flow distribution by the inlet manifold. Pressure and flow distributions for the full and 1/3rd width cases are compared using the Plates geometry, Figure 2b, at 1 m/s nominal cross-flow velocity, which was previously studied (Dal-Cin et al., 2006). Reynolds numbers in the channels, based on the average channel velocity predicted by the CFD solution, ranged from 170 to 470.

Changes in the flow distribution were minor when comparing predictions of the CFD solutions for the full width and 1/3rd width, Table 3. The flow maldistribution for the manifold itself was minor with κ_{man} = 1.41, accounting for the small differences between the full and 1/3rd width predictions. 1D predictions also compare reasonably well. The flow out each collector was nearly identical for all the module designs, hence we can postulate that flow distributions predicted by full and 1/3rd width solutions would be similar for the other designs.

Predicted pressure distributions along the distributor's centre lines were higher in the centre distributor compared to the side distributors in the last two channels, Figure 5. The abscissa intervals of 0.00635 m were used to identify transitions between the frames (channels) and plates. The larger flow in the centre distributor, coupled with the greater proportion of flow (54%) in the last two channels, resulted in a greater fluid deceleration and therefore pressure increase. The pressure changes along the distributor are dominated by the fluid decelerations, $\frac{1}{2}\rho(V_t^2 - V_{t-1}^2)$, where the downstream velocity $V_t < V_{t-1}$ (Dal-Cin et al., 2006). Frictional losses are negligible due to the short lengths (0.00635 m).

The pressure distribution in the distributor predicted by the 1/3rd width simulation lies between the pressure distributions for the centre and side distributors, shown by lines in Figure 5. This is not unexpected since the flow rate in the 1/3rd width simulation is also between that of the centre and side distributors. Collector pressure distributions are essentially identical, the flow in each of the three collectors in the full width, the 1/3rd width and 1D model were essentially the same.

The 1D model pressure distributions (□ and △) are qualitatively similar to the CFD values but are approximately 33% lower in the worst case. When the 1D model uses a nominal cross- flow velocity of 1.25 m/s, corresponding to the flow in the centre distributor, the pressure distribution in the distributor (▲) approaches that of the CFD solution. The assignment of a flow to the centre distributor was based on the dividing the manifold into three equal areas. The pressure distribution in the collector (■) is now overestimated, but this would be expected as the flow is higher than in the CFD simulations.

Table 3. Comparison of flow distributions (m/s) predicted by CFD for the full width, 1/3rd width and 1D solutions using the plate design at 1 m/s nominal cross-flow velocity

Solution	Channel Number					κ_{chan}
	1	2	3	4	5	
CFD Full Width	0.53	0.81	0.97	1.19	1.49	2.80
CFD 1/3rd	0.63	0.79	0.95	1.17	1.46	2.31
1D 1/3rd	0.55	0.75	0.99	1.24	1.47	2.68

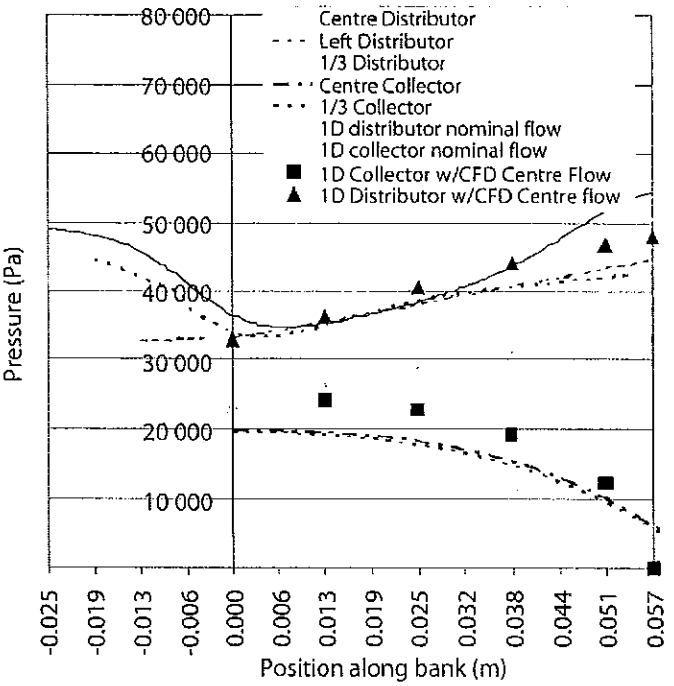

Figure 5. Pressure distributions for simulations on the full module width and 1/3rd width. Plate design. Lines represent CFD solutions, open symbols are 1D predictions with perfect inlet manifold distribution, solid symbols represent 1D solutions using flowrates calculated by CFD to centre distributor.

In summary, predictions of the flow distribution in the first bank of the plate and frame ultrafiltration module were nearly identical for CFD simulations based on the full width and 1/3rd width in the plate design. The maldistribution of the inlet manifold generated a higher pressure increase along the centre distributor as a function of increasing channel number compared to the 1/3rd width simulations. In the current design approach, assuming an equal feed to the distributors and symmetry with one third of the channel width is reasonable with respect to flow distributions and represents only one sixth of the computational demand of the full width case. The effect of the inlet manifold on flow distribution will be discussed further when evaluating alternative designs, as will its impact on pressure distribution predictions in the full module compared to considering only the first bank.

Original Design

The CFD predicted flow distributions for the full module width of the original design is shown in Figure 6 for 0.5, 1, 2, 3 and

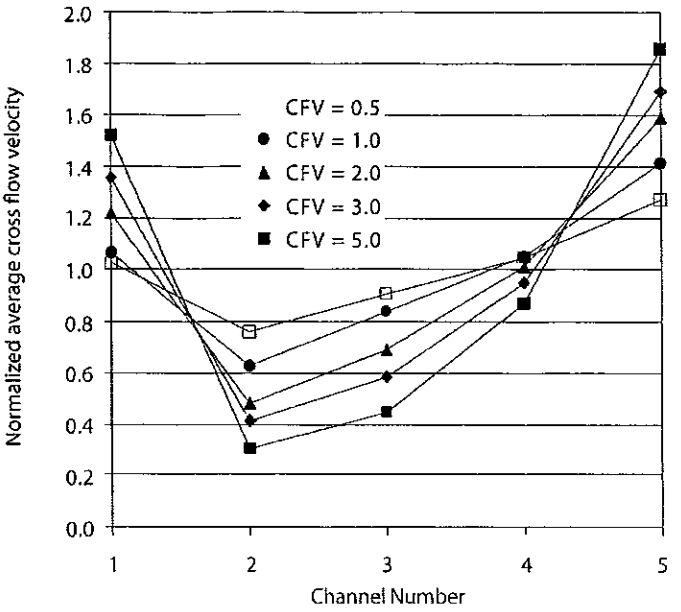

Figure 6. Normalized average cross-flow velocity distribution for the original module design as a function of channel number and design cross-flow velocity.

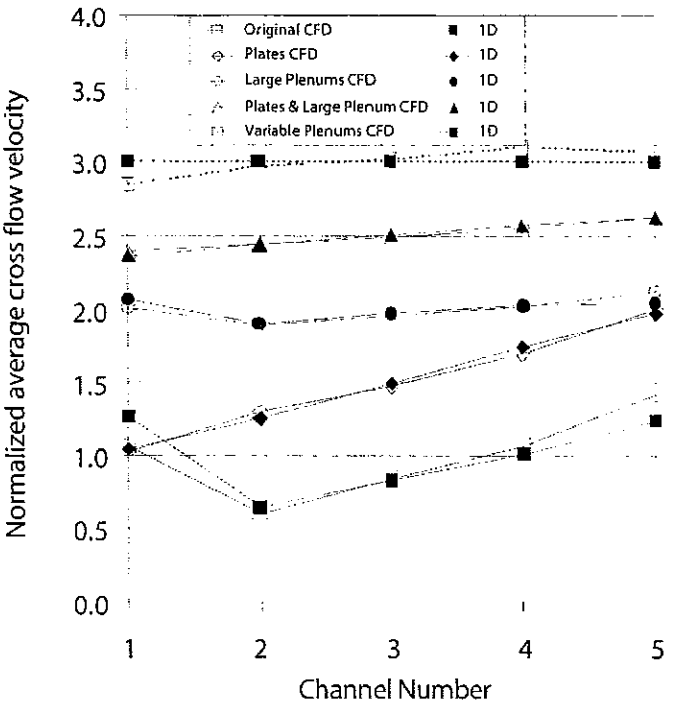

Figure 7. CFD (solid symbols) and 1D (closed symbols) predictions of the flow distribution for the different module designs at 1 m/s nominal cross-flow velocity. Flow distributions for each design are separated by adding 0.5, 1, 1.5 and 2.0 to the actual values.

5 m/s nominal design cross-flow velocities. Given the maldistribution that was determined at the different operating flow rates, Reynolds numbers ranged from 120 to 200 at 0.5 m/s, 200 to 440 at 1 m/s, 300 to 1 000 at 2 m/s, 380 to 1 580 at 3 m/s and 470 to 2 890 at 5 m/s. Increasing the design cross-flow velocities worsened the maldistribution, with κ_{chan} increasing from 1.7 to 6.1 at 0.5 and 5 m/s respectively for the CFD predictions. 1D simulations on 1/3rd of the module width were similar, with κ_{chan} ranging from 1.48 to 5.41. In the original design a parabolic distribution was predicted at all cross-flow velocities, with the minimum in the second channel. The parabolic nature of the flow distribution was the result of a frame as the first and last elements in the bank, yielding an orifice area for the first and last channels approximately 3.8 times larger than that of channels 2, 3 and 4, biasing the flow to the first channel.

Parabolic flow distributions were also predicted by others (Heggs and Scheidat, 1992 and Edwards et al., 1984) but for designs with constant plenum/orifice dimensions. 1D simulations in our previous work on 1/3rd of the module width and with constant orifice diameters in both plenums, only predicted parabolic flow distributions before incorporating the 1/7th power law velocity distribution, a variable contraction coefficient for the distributor and using the new modelling approach for combining flows in collector.

The impact of the flow maldistribution on the overall productivity of the bank was discussed qualitatively in Dal-Cin et al. (2006). In summary, if the flux is mass transfer limited throughout a bank, there will be almost no effect on the overall mass transfer coefficient for a bank as predicted by film theory. If the flux was expected to be pressure limited then the impact of the maldistribution can be such that the channels with less flow become mass transfer limited; impacting on the flux and separation of solutes. Response to changes in operating conditions, such as the pressure or the nominal cross-flow velocity can have unexpected results. Modelling flux and retention behaviour is beyond the scope of this work, but it is clear that a design with better flow distribution is desirable.

Alternative Designs

Flow maldistribution in channels

The parabolic flow distribution in the channels for the original design was attributed to the different orifice areas in channels 1 and 5 resulting from the use of frame elements at the front and end of the bank. An obvious modification to the module design would be to incorporate plate elements in these positions, thereby generating a module with constant dimensions for the plenums for each channel. This geometry was already discussed in the Comparison of 1/3rd and Full Width Simulations section. The flow distributions for this and the other designs are shown in Figure 7 at a design cross-flow velocity of 1 m/s. Channel Reynolds numbers for the alternative designs were between 260 and 360. Using a plate element at the start and end of the bank eliminated the parabolic nature of the flow distribution, however the overall maldistribution worsened with κ_{chan} increasing from 2.34 to 2.80.

Enlarging the plenum diameters to 0.0508 m yielded a significantly better flow distribution; κ_{chan} decreased to 1.25 and 1.26 for the two large tube designs with and without the plates respectively. The flow distribution in the design without the plate elements at the module ends has a minimum in the second channel and the design with plates throughout increases monotonically with channel number. The smaller velocity/pressure changes in the plenums yielded smaller pressure changes in the distributor and collector. Changes in the theoretical distributor pressure rise can be estimated from the kinetic energy term $\frac{1}{2}\frac{V^2_{centre\,line}}{\rho}$. Consider the comparison of the CFD centre distributor pressure increase for the Plate versus Plate and Big Plenums designs, Table 4. The diameter increase from 0.038

Table 4. Comparison of the distributor pressure increase predictions by the kinetic energy term in Bernoulli's equation and CFD at 1 m/s nominal cross-flow velocity

Configuration	Average inlet velocity in distributor (m/s)	Centre line velocity (m/s)	$\frac{1}{2}\frac{V^2_{centre\,line}}{\rho}$ (kPa)	ΔP_{CFD} (kPa)
Plate	5.30	6.49	18.5	17.8
Plate and Big Plenums	3.40	4.16	7.6	7.0

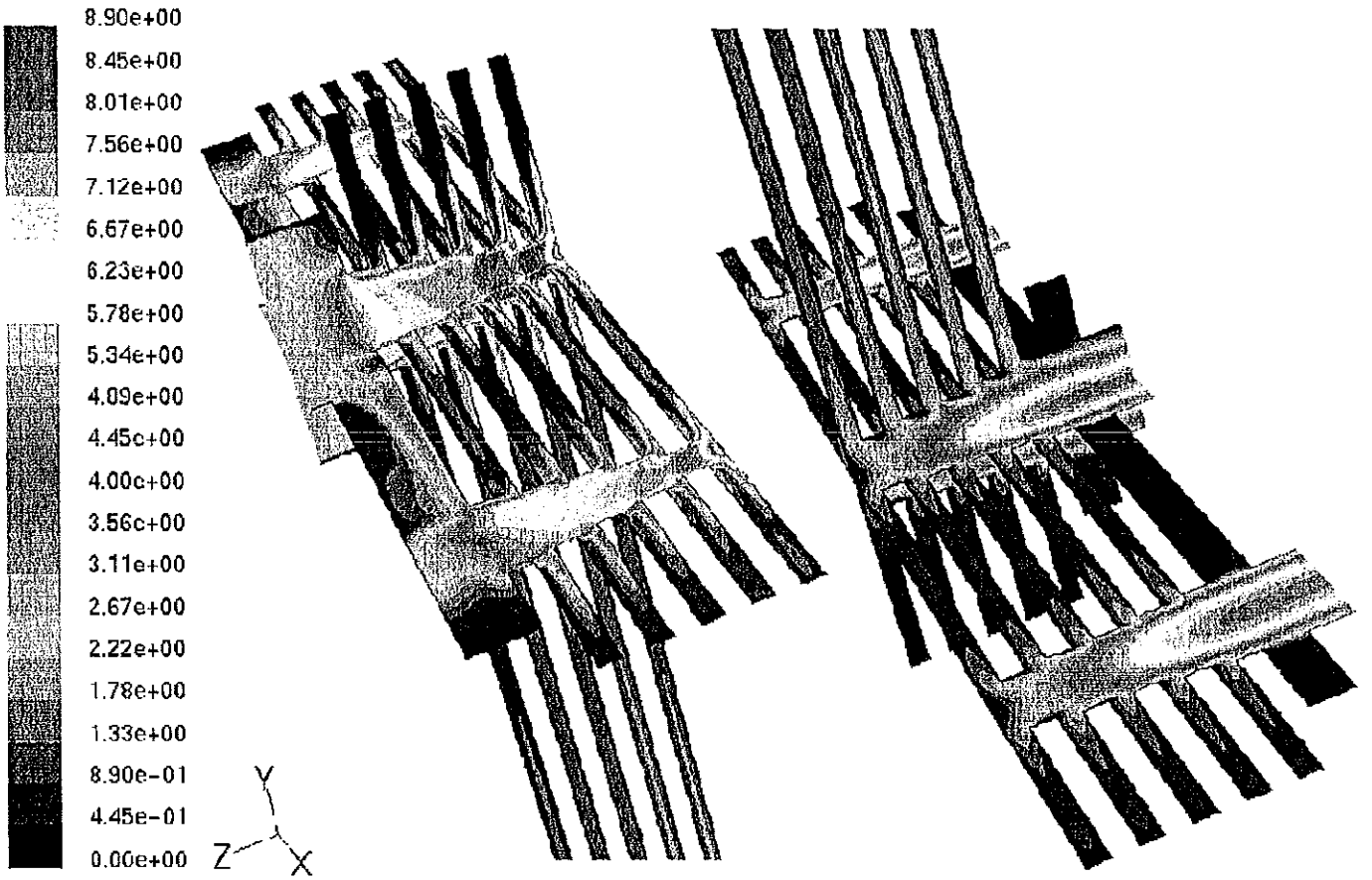

Figure 8. Velocity contours for the module design using variable distributor and collector diameters with a plate at the start and end of the bank

to 0.0508 m decreased the pressure rise from 17.8 kPa to 7.0 kPa. This diameter change represented a 2.11 times greater area, the pressure rise should have decreased by the square of this value. The difference can be accounted for by the different maldistribution in the two configurations giving different average velocities at the centre distributor inlet. Using the centre line velocity based on a $1/7^{th}$ power law velocity distribution, 60/49 $V_{average}$, the predicted pressure increases agree reasonably well.

Larger plenums have a reduced pressure maldistribution, which helps equalize the flow distribution in the channels. Simultaneously, the orifice area is coupled to the plenum diameter in the current design approach. The larger orifice areas in the distributor and collector can increase maldistribution by reducing the pressure drop in the channels that act as flow equilibrators. In this situation, reducing the pressure changes along the plenums was more important for achieving more uniform flow distribution.

The 1D optimization for the Variable Plenums case generated a design that yielded an increasing velocity in both the distributor and collector, Figure 8. The flow distribution was greatly improved over the original design but at the expense of a higher overall pressure drop.

The 1D model provided very good predictions of the flow distributions, based on comparisons to the CFD simulations, for all five module designs.

Pressure losses and distributions

Overall bank pressure drops

The overall pressure drop for the inlet manifold and bank was greatest for the variable diameter design, Table 2. The decreasing distributor diameter and smaller orifice areas contributed to more uniform flow but with corresponding increases in the orifice pressure losses, and therefore the overall bank pressure losses.

Overall pressure drops for the remaining designs followed expected patterns: the Original and Plate designs were lower than the Variable Plenum design as a result of the larger plenums throughout bank. The pressure drop with the Plate design was approximately 9.2 kPa greater than the Original design because of the additional contraction immediately after the inlet manifold

and at the bank outlet. The two large plenum designs had the lowest overall pressure drop with the additional plate adding a smaller loss, 2.4 kPa vs 9.2 kPa, because of the larger distributor after the inlet manifold.

The pressure drop for the repeating unit, the bank alone leading to an inlet at the next bank, can be estimated by subtracting the manifold losses for each design. The trend is the same as the when the inlet manifold was included. The bank losses may be biased by the effect of the inlet manifold maldistribution just as the inlet manifold losses were influenced by the bank design as will be discussed next.

Inlet manifold pressure losses

The inlet manifold flow distribution was demonstrated to be inadequate for most of the module designs. The manifold used was an easily manufactured and very compact item; it was a directional baffle located between the banks. The manifold pressure drops for the different designs are summarized in Table 2 and it is apparent that the manifold losses differ appreciably. The pressure losses are taken from the pressure profiles at the centre line of the main feed tube, manifold and centre distributor, from the inlet across the 0.01905 m depth of the manifold. In the designs with a plate immediately after the manifold, pressure losses along the 0.00635 m representing the plate are not included as this is part of the bank.

Pressure losses were negligible with the Large Plenum design and approximately 8 kPa for the two designs using a plate after the inlet manifold and small plenums, the greater loss being attributed to the fluid accelerating to enter the distributor and turbulent contraction losses. The manifold losses for the two remaining designs, the Original and Plate and Large Plenum, were 1.5 and 2.3 kPa respectively. The relatively low manifold pressure drop with the Original design with small plenums and no plate was the result of the large area for the first distributor, $1/3^{rd}$ of the inlet manifold area, Equation 2. Optimization of the manifold and bank design would have to be simultaneous because of the dependence of the manifold losses on the downstream conditions.

Optimizing the design of the inlet manifold is always beneficial but it represents a one time pressure loss, compared to the cumulative losses in the module for repeating bank designs. Furthermore, the flow distribution across the channel width was uniform almost immediately after entering the channel. The flow distribution to the second and presumably subsequent banks was nearly perfect. This suggests that future work can be reduced to $1/3^{rd}$ of the module width when considering the second bank onwards. Indeed, the effect of the inlet manifold may have biased the results in the current work with respect to the pressure losses for the repeating bank and design efforts should concentrate on the second bank and onwards where uniform flow distribution to the distributors can be assumed.

Plenum pressure distributions

1D pressure distributions in the distributor and collector in previous work (Dal-Cin et al., 2006) where $1/3^{rd}$ of the module width was modelled agreed qualitatively with CFD predictions but generally under-predicted the overall pressure. Pressures were under-predicted to a greater extent by the 1D model in the current work in comparison to the CFD simulations. This was attributed to the maldistribution of the inlet manifold which biased flow to the centre distributor, Comparison of $1/3^{rd}$ and Full Width Simulations section.

The greatest deviation between the CFD and 1D solutions (open symbols) was seen with the large plenum design, which had the largest κ_{man}, Figure 9. 1D model predictions of the pressure distribution using the flow to the centre distributor predicted by the CFD simulation was the equivalent of a 2.54 m/s nominal cross-flow velocity and grossly overestimated the pressure in the distributor.

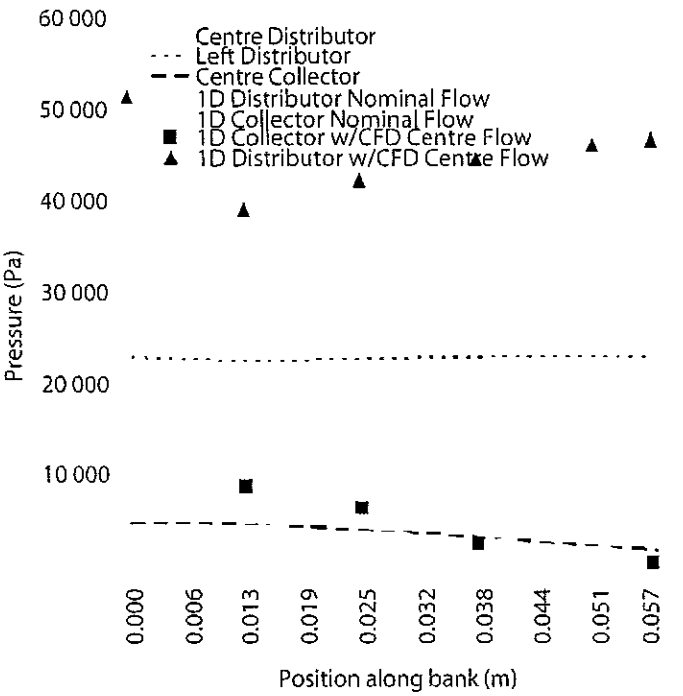

Figure 9. Pressure distribution in the distributor and collector in module design using large (0.0508 m) plenums. Lines represent CFD solutions, open symbols are 1D predictions with perfect inlet manifold distribution, solid symbols represent 1D solutions using flowrates calculated by CFD to centre distributor.

The variable plenum design was a unique case as the distributor diameter decreased and the collector diameter increased with increasing channel number. The 1D predictions for the diameter profile of the distributor were such that the smaller diameters generated an accelerating fluid and, thereby, a decreasing pressure, Figure 10. The rapid increase in the last channel is the result of the velocity fluid going to zero, this was not significant in any of the other designs because of the lower fluid velocity in the last distributor.

The best agreement was observed with the variable plenum design, Figure 10, which had the lowest κ_{man}. The 1D simulation, using the CFD centre tube flow, yielded pressure distributions quantitatively similar to the CFD predictions and was likely more accurate because of the relatively small correction for the manifold maldistribution. Similar observations were made for the other designs using a plate immediately after the inlet manifold.

Membrane pressure distributions

The pressure in the channels will be of greatest importance with respect to membrane performance rather than the pressure in the plenums. The pressure at the halfway point along the channel length is shown in Figure 11. Pressures were constant across the module width for all designs. The Variable Plenum design once again had the least favourable conditions, decreasing from 37 to 16 kPa, or a range of 21 kPa or approximately 38% of the bank pressure drop. The pressure range in the

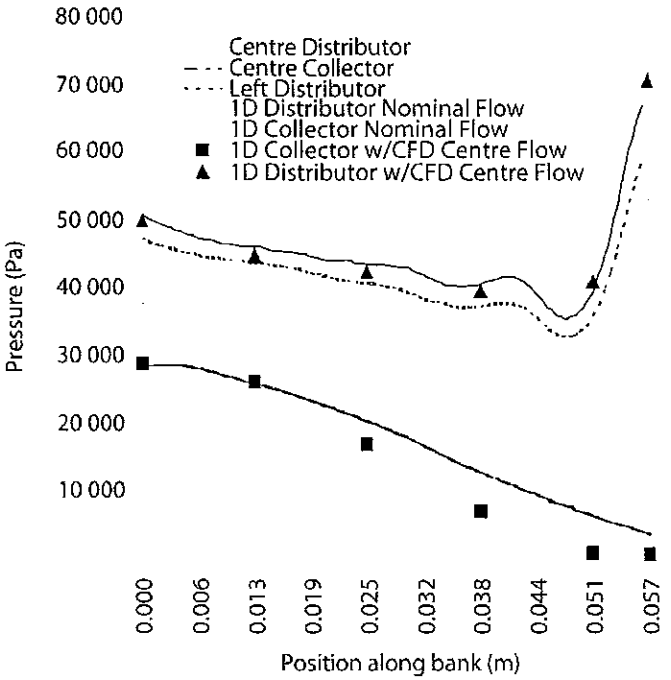

Figure 10. Pressure distribution in the distributor and collector in module design using large (0.0508 m) plenums. Lines represent CFD solutions, open symbols are 1D predictions with perfect inlet manifold distribution, solid symbols represent 1D solutions using flowrates calculated by CFD to centre distributor.

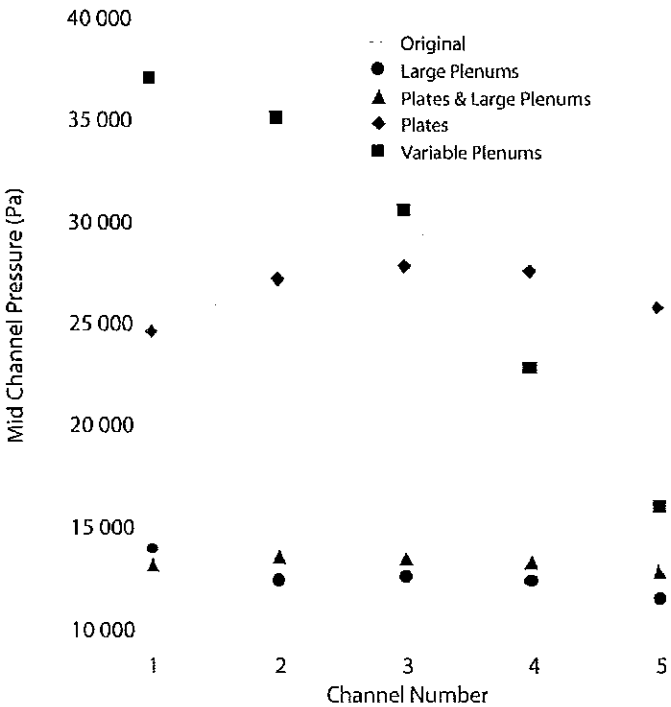

Figure 11. Pressure distributions in each channel at the half length point for all module configurations

Original design was 8 kPa and less than 3 kPa in the other designs.

The practical impact of these pressure distributions in the channels will be of minor concern in a full scale module. If the discharge pressure is set to a typical 500 kPa for used motor oil recovery, the pressure variation in the bank will be only 4.2% for the Variable Plenum design, in the last bank. The bank pressure drop for the Plate and Large Plenum design was approximately 24 kPa, giving approximately 240 kPa as the overall module pressure drop and 740 kPa at the inlet further reducing the impact of pressure variations within a bank.

Membrane modules may be operated at or near the mass transfer limited range in the last bank to maximize the module output. In this scenario, the changing transmembrane pressure in a bank, and the entire module, is of minor importance. Flow and pressure distributions will be more important if the module is to be operated below the "critical flux," where long term stable fluxes can be observed (Howell, 1995 and Nuortila-Jokinen et al., 2003).

OVERVIEW

The design that incorporated plates at the start and end of the banks, with the larger diameter plenums, was the best from several perspectives:

- most uniform flow distribution;
- lowest module pressure drop;
- most uniform pressure distribution in channels;
- simplest design (compared to variable diameter design);
- increased permeation area.

CONCLUSIONS

Flow and pressure distributions were simulated in a plate and frame ultrafiltration module with 5 channels operating in Z flow. Solutions were obtained using computational fluid dynamics to solve the Navier-Stokes equations and a one-dimensional model using Bernoulli energy balances. Solutions from CFD simulations in previous work on 1/3rd of the width of a plate and frame ultrafiltration module were extended to the full width of the module to include any effects of the inlet manifold. Changes to the flow and pressure distributions were minor for the module design using plates at the start and end of a bank.

Simulations with the original design predicted a parabolic flow distribution. This was attributed to the different orifice diameters in the first and last channels. Flow maldistribution, as measured by the ratio of the maximum/minimum flow in the 5 channels was 2.3 at a design cross-flow velocity of 1 m/s; indicating the need for an improved module design. Both solution methods identified fluid deceleration as generating a pressure increase along the distributor and fluid accelerations in the collector as generating pressure decreases. Coupled, these factors biased the greatest pressure drop and flow to the last channel.

Several designs were evaluated; the most effective was one using larger plenum diameters and a plate at the start and end of the bank. The flow maldistribution in the channels was reduced from 2.3 to 1.26, largely attributed to the reduced changes in the fluid velocity in the plenums. The manifold maldistribution was also reduced from 6.2 to 2.7, primarily by incorporating a plate, instead of a frame, at the inlet manifold discharge. This design also increased the permeation area, yielded the lowest bank pressure drop, most uniform pressure in the channels in a bank and could be readily retrofitted to existing modules.

Pressure and flow maldistributions resulting from the inlet manifold were not significant. Flow distributions across the width of a channel quickly equilibrated, within 0.1–0.2 m, and were smaller than the variations between different channels. Subsequent banks should see more uniform flow distributions as

the collectors, which become the distributors in the next bank, had equal flow.

Membrane performance will depend on the pressure in a channel rather than the plenums. The pressure maldistribution within a bank could be significant relative to the bank pressure drop, but will be considerably lower when the overall module pressure drop and outlet pressure are taken into account.

NOMENCLATURE

A	area (m^2)
C_c	contraction co-efficient (–)
d	orifice diameter
D_p	diameter (m)
D_h	hydraulic diameter, 4 × (flow area/wetted perimeter) (m)
e	orifice length (m)
h	channel gap (m)
L_p	plate thickness (m)
l	channel length (m)
n	number of collectors/distributors per bank
P	pressure (Pa)
V	average fluid velocity (m/s)
w	channel width (m)

Greek letters

μ	viscosity (kg/m/s)
ρ	density (kg/m^3)

Subscripts

c	collector
cc	fluid entering collector at outer annulus
co	collector orifice
cr	fluid existing in collector
d	distributor
dc	fluid leaving distributor outer annulus
dr	fluid remaining in distributor
do	distributor orifice
o	orifice

REFERENCES

Chen, C.-W., Y.-W. Shau and C.-P.Wu, "Analogic Modelling for Systemic Circulation," Biomed. Eng. Appl. Basis Commun. 8(2), 145–150 (1996).

Cui, X.-Z. and K.-Y Kim, "Three Dimensional Analysis of Turbulent Heat Transfer and Flow through Mixing Vane in a Subchannel of Nuclear Reactor," J. Nucl. Sci. Technol. 40(10), 719–724 (2003).

Dal-Cin, M. M., K. Darcovich, M. Bourdoncle, Z. Khan and D. Caza, "Comparison of CFD and One-Dimensional Bernoulli Solutions of the Flow in a Plate and Frame Ultrafiltration Module in Z Configuration," J. Membr. Sci. 268(1), 74–85 (2006).

Edwards, M. F., D. I. Ellis and M. Amooie-Foumeny, "The Flow Distribution in Plate Heat Exchangers," in "Heat Transfer," Vol. 1, IChemE, Symposium Series, 86 (1984), pp. 1289–1302.

Heggs, P. J. and H.-J. Scheidat, "Thermal Performance of Plate Heat Exchangers with Flow Maldistribution," HTD-Vol. 201, Compact Heat Exchangers for Power and Process Industries, ASME (1992), pp. 87–93 .

Howell, J. A. "Subcritical Flux Operation of Microfiltration," J. Membr. Sci. 107(1–2), 165–171 (1995).

Jones, G. F., "Heat Transfer and Flow Distribution Within Radiant-Convective Finned-Tube Manifold Assemblies," PhD Thesis, University of Pennsylvania (1981).

Karode, S. K., "Laminar Flow in Channels with Porous Walls, Revisited," J. Membr. Sci. 191, 237–241 (2001).

Ke, S. L. and H. C. Ti, "Transient Analysis of Isothermal Gas Flow in Pipeline Network," Chem. Eng. J. 76, 169–177 (2000).

Kee, R.J., P. Korada, K. Walters and M. Pavol, "A Generalized Model of the Flow Distribution in Channel Networks of Planar Fuel Cells," J. Power Sources 109, 148–159 (2002).

Launder, B. E. and D. B. Spalding, "Lectures in Mathematical Models of Turbulence," Academic Press, London, England (1972).

Majumdar, A. K. "Mathematical Modelling of Flows in Dividing and Combining Flow Manifold," Appl. Math. Mod. 4(12), 424–432 (1980).

Manna, M. and A. Vacca, "Scaling Properties of Turbulent Pipe Flow at Low Reynolds Number," Comput. Fluids 30, 393–415 (2001).

Miranda, J. M.and J. B. L. M. Campos, "An Improved Numerical Scheme to Study Mass Transfer over a Separation Membrane," J. Membr. Sci. 188, 4959 (2001).

Nuortila-Jokinen, J.; M. Mänttäri, M. Nyström, "The Pulp and Paper Industry," in "Membranes for Industrial Wastewater Recovery and Re-Use," S. Judd, and B. Jefferson, Eds., Elsevier Advanced Technology, Kidlington, Oxford, U.K. (2003), pp. 102–131.

Rokni, M. and B. Sundén, "Performance of RNG Turbulence Modelling for Forced Convective Heat Transfer in Ducts," Int. J. Comput. Fluid D. 11, 351–362 (1999).

Toldy, F., A. Bitai, G. Lipovszki and P. Niedermayer, "Checking and Control of Pipeline Networks," Periodica Polytechnica, Mech. Eng. 22(4), 313–323 (1978).

Tsitlik, J. E., H. R. Halperin, A.-S. Popel, A. A. Shoukas, F. C. P. Yin and N. Westerhof, "Modelling the Circulation with Three-Terminal Electrical Networks Containing Special Nonlinear Capacitors," Ann. Biomed. Eng. 20, 595–616 (1992).

Manuscript received August 29, 2005; revised manuscript received December 9, 2005; accepted for publication February 9, 2006.